ORIGINAL PAPER

Pulsed Aerosol-Assisted Low-Pressure Plasma for Thin-Film Deposition

G. Carnide[1,2] · C. Simonnet[1,3] · D. Parmar[1,2] · Z. Zavvou[1,2] · H. Klein[1,2] · R. Conan[1] ·
V. Pozsgay[1] · T. Verdier[1] · C. Villeneuve-Faure[1] · M. L. Kahn[2] · L. Stafford[3] ·
R. Clergereaux[1]

Abstract

Plasma-enhanced chemical vapor deposition is a well-developed technique that is commonly applied in the preparation of thin films. However, this technique is limited to thermodynamically stable and chemically inert precursor gases or vapors. Recently, pulsed aerosol-assisted plasma processes have emerged as an advantageous alternative that allows for the injection of various liquid solutions in the plasma, regardless of their properties. This study examines the production of thin films by pulsed injection of pentane aerosols into a low-pressure RF capacitively coupled plasma. This technique produces thin films with high material balance and a high degree of control by adjusting the pulsed injection parameters. At the pulse scale, pulsed injection induces a temporary increase in the working pressure, resulting in time-dependent mechanisms that can affect the dynamics of thin-film deposition at the process scale. Overall, the results show a key role of droplets and their kinetics (ballistic transport, vaporization kinetics, electrostatic confinement). Hence, to efficiently apply this method in the preparation of (multi-)functional coatings, the aerosol must be carefully characterized.

G. Carnide, C. Simonnet, D. Parmar, Z. Zavvou have contributed equally.

✉ R. Clergereaux
richard.clergereaux@laplace.univ-tlse.fr

1   Laplace - Laboratoire Plasma Et Conversion d'Energie, 118 Route de Narbonne, 31062 Toulouse Cedex 9, France

2   LCC - Laboratoire de Chimie de Coordination CNRS, 205 Route de Narbonne, 31077 Toulouse Cedex 4, France

3   Département de Physique, UdeM - Université de Montréal, Montreal, QC H3C 3J7, Canada

Introduction

Plasma-enhanced chemical vapor deposition (PE-CVD) is often used to prepare thin films at low temperature in a controlled manner [1, 2]. The deposition proceeds via the decomposition of precursor molecules upon inelastic collisions with plasma electrons and the recombination of the resulting reactive species on surfaces. For example, in methane (CH_4) plasmas, the molecules are decomposed into radicals (*e.g.* $CH_3^{°}$) and ions (*e.g.* CH_3^{+}) that recombine on surfaces to form so-called diamond-like carbon (DLC) thin films [3, 4]. These films are commonly used to protect functional surfaces against wear, friction, and other tribological phenomena [5, 6].

Thin film growth mechanisms are dependent on the process conditions (*e.g.* pressure, excitation frequency, and reactor geometry), plasma parameters (*e.g.* electron temperature, plasma density, and radical density), and the properties of species reacting on the walls. For instance, DLC materials are usually obtained in low-pressure asymmetrical RF plasmas using the high ion bombardment developed in these devices [3, 5, 7–9].

However, these processes are not really efficient. Indeed, in these different works focused on CH_4, the deposition rate varies between 0.5 and 50 nm.min^{-1}. Divided by the gas flow rate, this yields a material balance (*i.e.* ratio of the deposition rate to the injected gas volume [10]) in the 0.1—3.5 nm / cm^3 range.

For a given experiment, the material balance can only be improved by increasing the deposition rate. Such optimization can be achieved by modifying the precursor structure as, for instance, by using larger alkanes such as ethane (C_2H_6), propane (C_3H_8), or butane (C_4H_{10}) [10, 11] or unsaturated precursors (alkenes and alkynes) [11]. For example, the deposition rate is improved in acetylene (C_2H_2) plasmas [16] even if additional dust particle growth mechanisms in the plasma volume can occur (as discussed in dusty plasmas [12]).

To further increase the material balance of the PE-CVD process, larger hydrocarbon molecules as pentane, n-hexane, cyclohexane, benzene, and toluene can be used. However, these molecules are liquid at room temperature. Hence, these compounds cannot be directly applied in PE-CVD. It requires a stage of injection by spraying, bubbling, nebulization, Direct Liquid Injection (DLI) [13], or fuel injection [14–18] followed by a stage of vaporization. Despite the effectiveness of the afore-mentioned techniques, they cannot be readily applied to deposit multifunctional thin films using slightly volatile liquids [19], liquid mixtures [20], liquid solutions with highly reactive molecules [21], or colloidal solutions [22–25].

Alternatively, liquids can be directly introduced into the plasma as an aerosol *i.e.* a suspension of micrometric liquid droplets in gaseous medium [26–29]. However, the continuous injection of droplets can lead to the formation of a misty plasma [30, 31], where, in analogy with dust particles [12], the presence of droplets can introduce additional electron losses due to electron attachment on the liquid particles upon droplet collision and further can modify the plasma process.

To minimize these impacts, Pulsed Direct Liquid Injection (PDLI) [13] is used instead. Although the pulsed injection temporarily affects the density of neutrals, a stationary state can be restored between pulses, and the plasma—actually, n_e and T_e—can return to steady state [32]. This optimizes the ionization rate and improves thin-film deposition [29]. PDLI allows for the injection of any liquid solution, regardless of its composition and thermodynamic properties. Moreover, it can be used to develop hybrid,
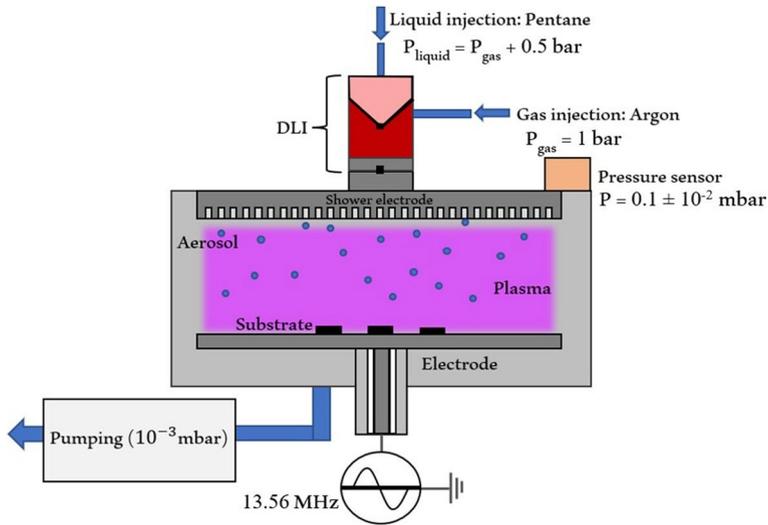
Fig. 1 Experimental setup

safer-by-design nanocomposite thin film deposition processes adapted to low- and atmospheric-pressure plasma conditions [29, 33].

Although PDLI has been successfully applied, the effects of the pulsed injection mode on process parameters remain poorly documented. In this study, we investigate the deposition of carbon-based thin films by PDLI in an asymmetric RF capacitive discharge, using pentane-argon aerosols. The characteristics of the aerosols are assessed, and their effects on the global process characteristics are discussed at the process and pulse scales. Notably, this work emphasizes a key role of liquid droplets evaporation on the final coating. The synergy between the dynamics of the pulsed aerosol and the plasma deposition process is analyzed.

Material and Methods

The process studied here consists in thin film deposition by injecting a pentane-argon aerosol in a RF discharge. As schematized in Fig. 1, the experimental chamber was a stainless-steel capacitively coupled plasma reactor equipped with two electrodes. The 30-cm-diameter electrode placed on the bottom was connected to a radio frequency generator (13.56 MHz) coupled to a matching box. As the chamber is grounded, the discharge was highly asymmetric capacitive system with a self-bias voltage on the bottom electrode.

A set of two pumps (a primary ADP and a secondary ROOTS vacuum) was used to pump the plasma chamber down to 10^{-3} mbar before each experiment. The Pulsed Direct Liquid Injection (PDLI) system was a two-stage injecting device purchased from Kemstream™. This device is commonly used in thermal CVD and ALD systems to supply precursor(s) and dispersions in pulsed mode [13]. In the first stage of injection, droplets of the liquid solution (here, pentane) were transferred from a pressurized liquid reservoir ($P_{liq} = 1.5$ bar above atmospheric pressure; reservoir pressurized with argon) to a mixing chamber through a liquid valve. The amount of transferred liquid was controlled by

adjusting the time (liquid injection opening time, t_{liq}) and frequency (injection frequency, f_{liq}) of valve opening. The liquid droplets in the pressurized mixing chamber were mixed with argon gas at $P_{gas} = 1$ bar above atmospheric pressure. In the second stage, the generated aerosols were introduced into the downstream process via an exhaust gas valve whose opening time (t_{gas}) and frequency (f_{gas}) can also be adjusted. Here, the PDLI system was connected to a shower head placed at 6 cm above the bottom electrode. For full characterization, the sprayed aerosols were evidenced by scattering a blue LED ($\lambda = 455$ nm) on the liquid droplets. Movies were recorded at 135° from the light beam using a high-speed Photron Ultima APX RS 3000 camera (4000 frames per second).

Plasma deposition was conducted using a Cesar 1310 RF generator from Dressler with an injection power set to 100 W and < 8 W maximal reflected power—automatic adjustment was activated on the matching box to maintain the discharge. To assess the effects of pulsed aerosol injection on the process, time variations of the pressure, injected power, and DC self-bias voltage were recorded on a WaveJet 334A oscilloscope using an ACC1009 relative gauge from Alcatel, the RF current and voltage profiles measured with a current–voltage probe from Solayl™, and the generator outputs, respectively.

Finally, the thickness and morphology of the thin films deposited on 1×1 cm^2 intrinsic silicon substrates placed on the bottom electrode were examined using mechanical profilometry (Tencor – Alpha Step IQ) and Atomic Force Microscopy (AFM BRUKER Multimode 8 in tapping mode) analyses.

Results

3.1 Mechanisms Involved in the Aerosol-Assisted Plasma Deposition Process

This section presents the characteristics of the pentane-argon aerosols injected at $t_{liq} = 5$ ms, $t_{gas} = 10$ ms, and $f_{liq} = f_{gas} = f = 0.1$ Hz, and of the coating deposited in such condition. The main mechanisms are studied at the process (from 1 to 20 min) and pulse period scales (10 s).

3.1.1 Characteristics of the Deposited Thin Films

First, coatings were deposited for different deposition times. As shown in Fig. 2a, the mean thickness increases linearly with time corresponding to an average deposition rate of 8.6 ± 0.1 nm.min^{-1}. Considering at $t_{liq} = 5$ ms, a volume injected per pulse of $q = 6$ μL, *i.e.*, at a pulse frequency of $f = 0.1$ Hz, a liquid flow rate of $Q_{liq} = 36$ μL.min^{-1}, the material balance, defined as the ratio of the deposition rate to the liquid flow rate, *i.e.* the volume of pentane injected per minute, is about 240 nm / cm^3, or, considering the film density of hydrogenated amorphous carbon in the 1.5–2 g/cm^3 range, about $4 \ 10^{-5}$ g / min cm^2 sccm. These values are really high compared to those reported in the literature [9], which indicates that the aerosol-assisted PE-CVD process used in this study is a really effective process for the deposition of thin films.

The carbon-film morphology was assessed by AFM. The film has a smooth surface ($R_a \approx 0.6$ nm / $R_q \approx 1.3$ nm over 5 μm×5 μm) with many defects (Fig. 2b). Indeed, on the matrix (darkened areas), nano-/micro-objects (in white) are observed dispersed on the

(a)

(b)

(c)
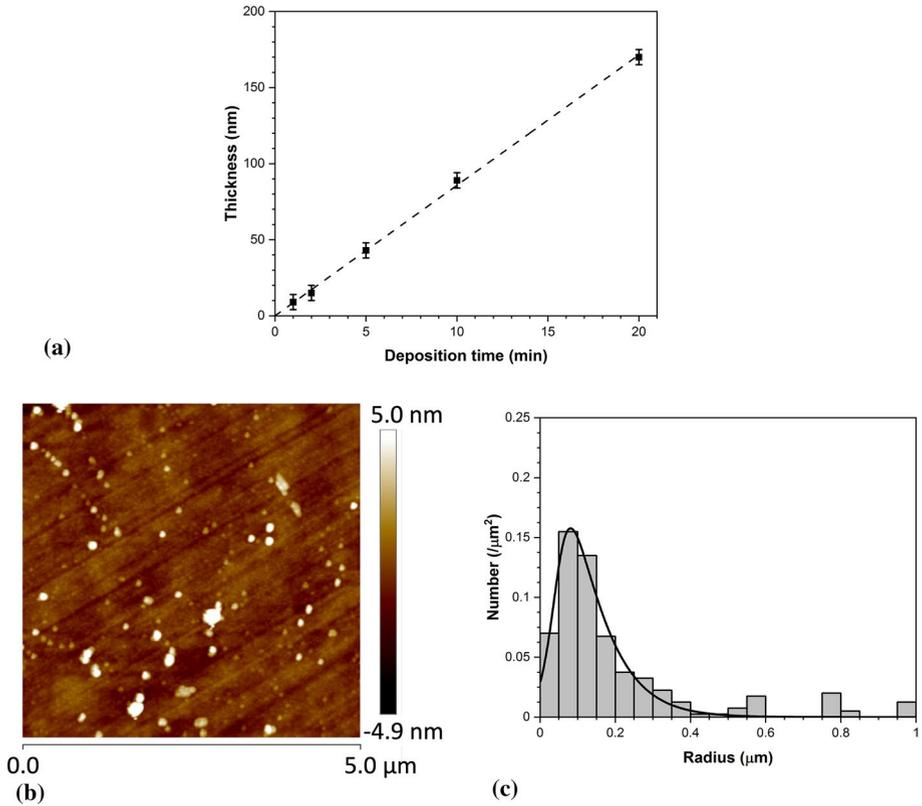
Fig. 2 Characteristics of the thin film obtained by plasma processing of the argon-pentane aerosols produced at $t_{liq}=5$ ms, $t_{gas}=10$ ms, and $f=0.1$ Hz. **a** Evolution of the average film thickness as a function of deposition time. **b** Typical AFM image of the coating deposited for 10 min and **c** the corresponding size distribution of the nano-objects observed by AFM

film surface. The dimensions of these objects were determined using ImageJ[1] on several images. The size distribution presented in Fig. 2c demonstrates that these objects have an average radius between 50 and 100 nm with extreme values up to few hundreds of nm.

These objects can not be assimilated to dust particles formed in the plasma volume and deposited on the substrate. Indeed, the time scale of dust particle growth (generally, of few minutes [34]) is much larger than that of the pulse scale (10 s). Therefore, they are more probably formed from the droplets injected in the plasma phase and reaching the substrate surface [35].

Hence, aerosol-assisted plasma deposition is an efficient process. It needs to be fully characterize. Indeed, the pulsed injection leads to temporal evolutions of the process parameters. The dynamics of the different mechanisms involved are estimated in the following.

---

[1] free software: https://imagej.nih.gov/ij/
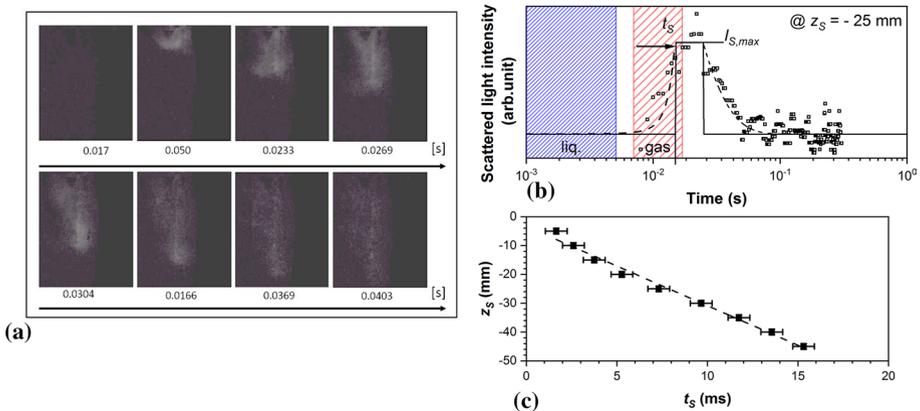
Fig. 3 **a** High-speed camera images of the argon-pentane aerosols ($t_{liq}=5$ ms, $t_{gas}=10$ ms, and $f=1$ Hz). **b** Temporal evolution of the scattered light intensity during a pulse (blue and red hatched areas represent the liquid and gas injection setpoints, respectively). **c** Evolution of the transit times, t_S, of the aerosols along the quartz tube. The slope of the linear curve corresponds to the average aerosol velocity

3.1.2 Characteristic Times of the Process

First, the aerosols were imaged directly at the exhaust of the PDLI by inserting a quartz tube between the injector and the shower head. The recorded images shown in Fig. 3a demonstrate that even at low-pressure ($7 \cdot 10^{-3}$ mbar), they comprise micrometric droplets scattering blue light beam.

The temporal evolution of the scattered light intensity was analyzed at various distances (z_S) from the PDLI. Figure 3b presents the profile measured at $z_S=-25$ mm from the PDLI. Clearly, it reproduces the rectangular function of pulsed injection. The delay in comparison with the PDLI settings (hatched areas in blue and red) of $t_S \approx 8$ ms is characteristic of the average velocity of the aerosols: t_S determined for different z_S, and plot as in Fig. 3c, reveals an average aerosol velocity of ≈ 2.7 m.s^{-1} (slope of the linear fit). Assuming that this velocity does not change without the quartz tube, *i.e.* when going from the PDLI to the plasma chamber, the liquid droplets travel the distance between the two electrodes of 6 cm in ≈ 22 ms. This value is used as a lower limit of the droplets residence time due to ballistic transport.

From the shower head to the bottom electrode, the droplets can undergo various processes. First, liquid vaporization can occur. This mechanism is reducing the droplet size by supplying the plasma chamber with vapors. In our case, full evaporation of the droplets does not occur within 40 ms, as evidenced by the presence of droplets over this full time scale in the fast camera movie (Fig. 3a). This value can be used as an underestimate of the evaporation time.

With their ballistic transport and evaporation, by analogy with dust particles [34], liquid droplets can charge by collecting electrons and ions from the plasma. Considering a low-pressure argon plasma with $T_e=1$ eV, $T_i=300$ K, and $n_e=n_i=10^{15}$ m^{-3} [34], it takes ≈ 10 µs to charge micrometric liquid droplets.

Charged, the droplets can be efficiently electrostatically confined above the sheath. The droplets can then further evaporate, heat up in the plasma, recombine in the plasma,
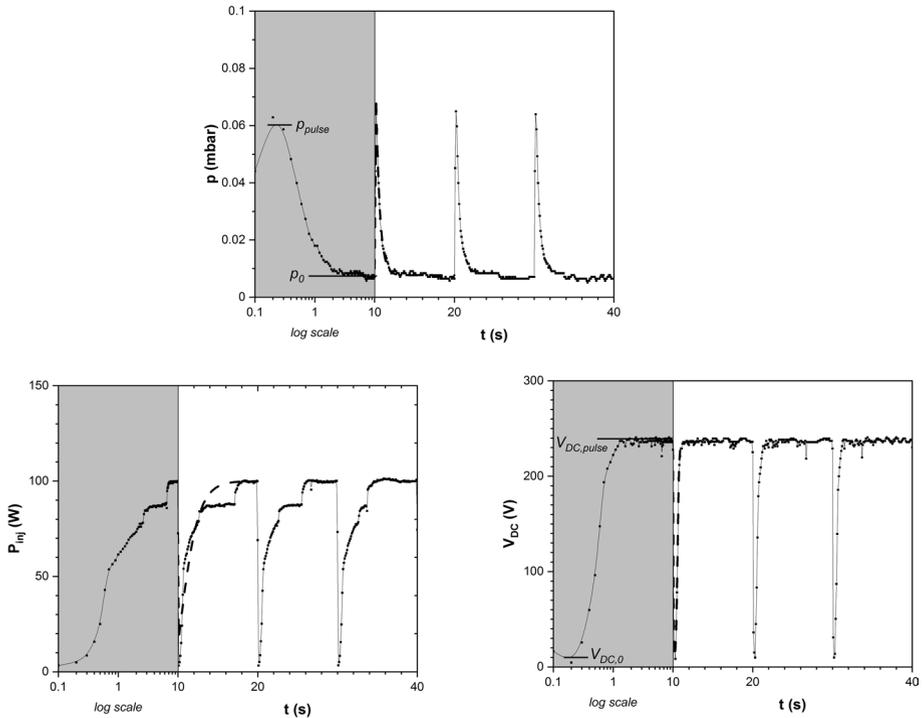
Fig. 4 Temporal evolution profiles of **a** the working pressure, **b** injected power and **c** self-bias voltage recorded at the pulse period scale ($t_{liq}=5$ ms, $t_{gas}=10$ ms, and $f=0.1$ Hz)

burst [30] or solidify [35]. The latter mechanism may explain the presence of nano-/microbjects on AFM images in the conditions investigated (Fig. 2b).

Conversely, the confinement of droplets also affect the plasma behaviors (power injection, electron density and temperature). To further discuss these different mechanisms, the temporal evolutions of the process parameters at the pulse period scale are investigated in the next section.

3.1.3 Temporal Evolutions at the Pulse Period Scale

The temporal evolution profiles of the working pressure, injected power, and self-bias voltage were recorded during the pulse period for the first 4 pulses (Fig. 4). As shown in Fig. 4a, pulsed injection induces significant variations in the plasma chamber pressure, with values sharply increasing from $p_0 \approx 7 \ 10^{-3}$ to $p_{pulse} \approx 6 \ 10^{-2}$ mbar at the beginning of the pulse, then gradually decreasing to p_0. Such temporal evolutions of the pressure are related to the transient balance between pulsed injection, pentane liquid droplets evaporation and continuous pumping [31, 32].

The pulse gas injection is smothering the discharge. Indeed, Fig. 4b shows sudden variations of the injected power from the initial set point at 100 W down to ≈ 2 W immediately after the pulse. This behavior observed in the initial increase in pressure is attributed to the collision frequency, altering the electron density, n_e, and temperature, T_e [36]. This is also observed on the self-bias voltage time evolutions with values droping from $V_{dc,0} \approx -240$ V
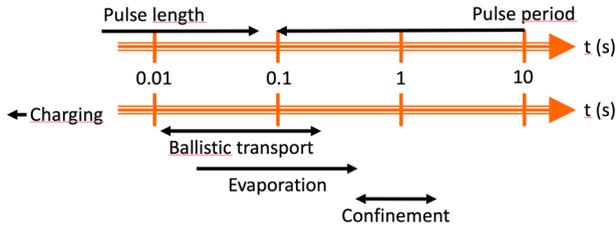
Fig. 5 Representation of the typical dynamical processes occurring in aerosol-assisted PE-CVD and their corresponding time domains

down to $V_{dc,pulse} \approx -9$ V during the pulse (Fig. 4c). After the pulse, both the injected power and the self-bias voltage return to their initial values. However, in contrast with the self-bias, the injected power exhibits a much longer return-to-steady state kinetics (of few s) with an intermediate steady state value around ≈ 85 W. The latter suggests that droplets are altering the discharge for, at least, few seconds. This confinement is attributed to electrostatic repulsion of the charged droplets in the plasma volume. The droplet lifetime in the plasma volume is then estimated in the second range.

As a summary, aerosol-assisted PE-CVD involves mechanisms with different dynamics (Fig. 5). Unlike the charging time, which is relatively short, the droplet ballistic transport, evaporation time, and lifetime in the plasma volume are in between the pulse length ($t_{liq} = 5$ ms) and the pulse period ($1/f = 10$ s). The deposition process may then depend to a great extent on the PDLI injection parameters. Their effects are discussed below.

4 Influence of the Injection Frequency, *f*

The impact of the injection frequency on thin film deposition was assessed in the range of 0.1–10 Hz, at the injection time, $t_{liq} = 5$ ms. Based on the representative time domains shown in Fig. 5, it means that the gas composition is renewed at a similar rate or faster than the droplets plasma lifetime and evaporation time.

4.1 At the Process Scale

First, as the gas flow injected per pulse, q, is constant at a given liquid opening time, t_{liq}, the injection flow rate, Q_{liq}, is a linear function of the injection frequency, f (Fig. 6a). However, the deposition rate at these different conditions, does not exhibit significant variations with an average value of 9.3 ± 0.8 nm.min^{-1}. Therefore, the material balance is inversely proportional to the injection frequency. In other words, the deposition process seems to be limited by the energy provided to the precursor, and not by the amount of precursor [36, 37].

In addition, from AFM images presented in Fig. 6b, the roughness of the deposited coating (R_a and R_q in the 1 nm range over 5 µm×5 µm) does not appreciably change with the frequency. However, the number of nano-/micro-objects is lowered at high frequency: when the pulse injection duration is equal to or less than the droplet lifetime in the plasma volume, these particles are no longer formed and deposited. This agrees well with the hypothesis of droplet confinement in the plasma volume for at least few seconds.

(a)

(b)
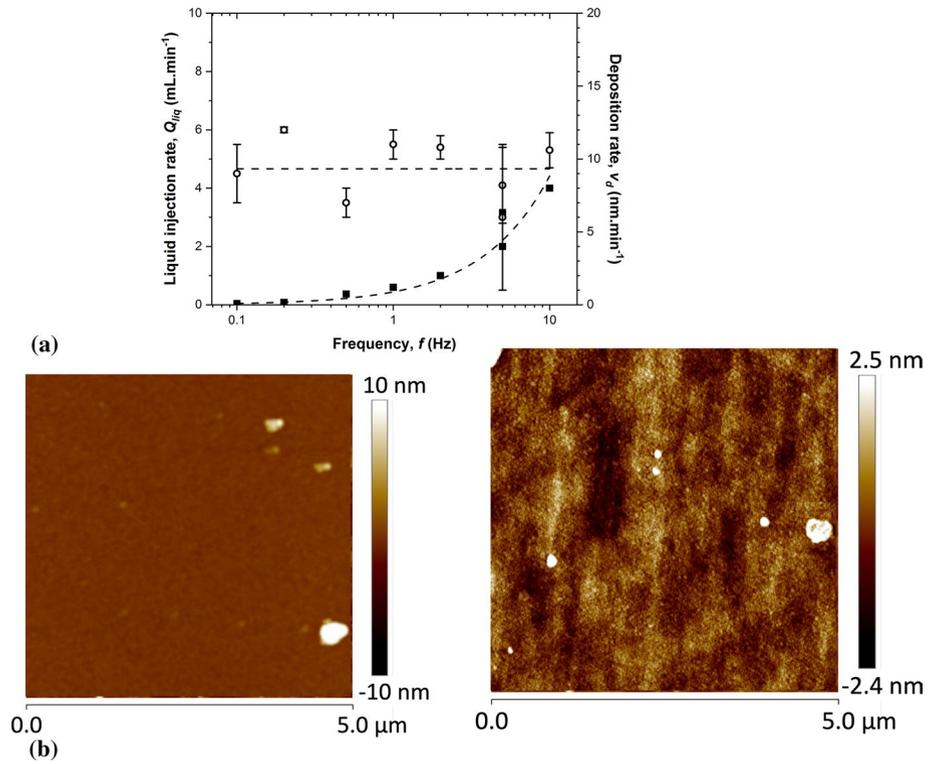
Fig. 6 **a** Variation of liquid injection rate (squares) and deposition rate (open circles) as a function of injection frequency in the range of 0.1–10 Hz. **b** AFM images of the coatings obtained at $f=1$ and 10 Hz ($t_{liq}=5$ ms and $t_{gas}=10$ ms)

a)   b)
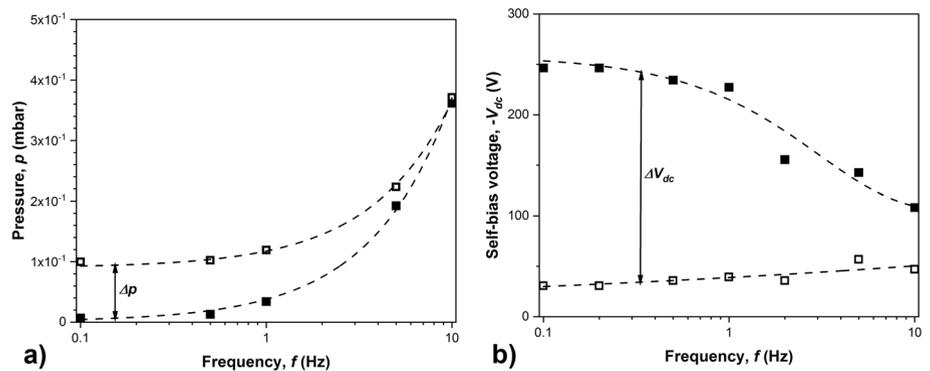
Fig. 7 Variations of **a** pressure and **b** self-bias voltage as a function of injection frequency ($t_{liq}=5$ ms)

4.2 At the Pulse Scale

The values of working pressure and self-bias voltage during the pulse and at steady state also vary with the frequency. As shown in Fig. 7a, both, p_0 and p_{pulse} increase with

f (by factors of ≈ 50 and ≈ 4, respectively, from 0.1 to 10 Hz); however, the difference $\Delta p = p_{pulse} - p_0$ decreases. As the pumping flow and the aerosol injected per pulse remain unchanged, it suggests that aerosol kinetics are modified upon increasing the number of pulse. While the evolution of p_0 with f is attributed to the balance between gas and pumping flows [26, 31], Δp can be relied to the liquid droplets evaporation, the droplets being incompletely evaporated at higher frequency. It thus reduces the density of neutral vapors in the plasma chamber. Hence, even if the liquid injection rate increases, the deposition rate can not further change. But in contrast with our previous discussion, the reduction of the material balance can not be attributed to energy deficit but to a reduced neutral vapor density.

Note that, with the evolution of the working pressure, the injection frequency modifies the self-bias voltage. As shown in Fig. 7b, the absolute value of $V_{dc,0}$ decreases by a factor ≈ 2 from 0.1 to 10 Hz while $V_{dc,pulse}$ remains practically unchanged. The phenomenon at steady state can be attributed to the variation of p_0 as typically reported in low-pressure plasmas [32, 38]. In contrast, the difference ΔV_{dc} suggests that the discharge is weakly altered by the pulsed injection at higher f and is only affected by the number of droplets injected per pulse.

Therefore, droplet evaporation in the plasma is the key mechanism for thin-film deposition. For a given quantity of liquid injected per pulse, an increase of the injection frequency highly limits the droplet lifetime compared to the evaporation and confinement times. Consequently, it reduces the density of neutrals formed through the evaporation of liquid droplets in the plasma volume. It also affects the formation and deposition of nano-/micro-objects, the latter resulting from by plasma-induced reactions on droplets confined in the volume.

# 5 Influence of the Liquid Injector Opening Time t_{liq}

In this section, we discuss the impact of injection time on the deposition process, in the range of 2–50 ms. This time range falls within the evaporation and ballistic transport times defined in Fig. 5. To limit the effects of liquid droplets confinement, the experiments are performed with an injection frequency fixed at 1 Hz.

5.1 At the Process Scale

Here, the quantity of liquid injected during a pulse, q, and, at a given f, the injection flow rate, Q_{liq}, vary linearly with t_{liq} (Fig. 8a). Considering that the droplet size does not change, it implies that the number of droplets is proportionnal to t_{liq}.

According to the previous discussion, with the number of droplets, the density of vapour due to droplets evaporation may increase and, consequently, the deposition rate and the material balance may be optimized. The latter looks true from $t_{liq} = 2$ to 10 ms. However, when the number of droplets is increased by a factor 5, the deposition rate only grown by a factor of ≈ 2 (from 8 to 14 nm.min^{-1} as shown in Fig. 8a). In addition, a saturation is reached beyond 10 ms. Hence, the variations of deposition and injection rates tend to reduce the material balance at higher t_{liq}, *i.e.* with the number of droplets.

Finally, in contrast with the frequency, the film morphology does not appreciably change with the liquid injection time. With a roughness of the coating still in the 1 nm range (over 5 μm × 5 μm), the presence of nano-/micro-objects dispersed on the film surface is
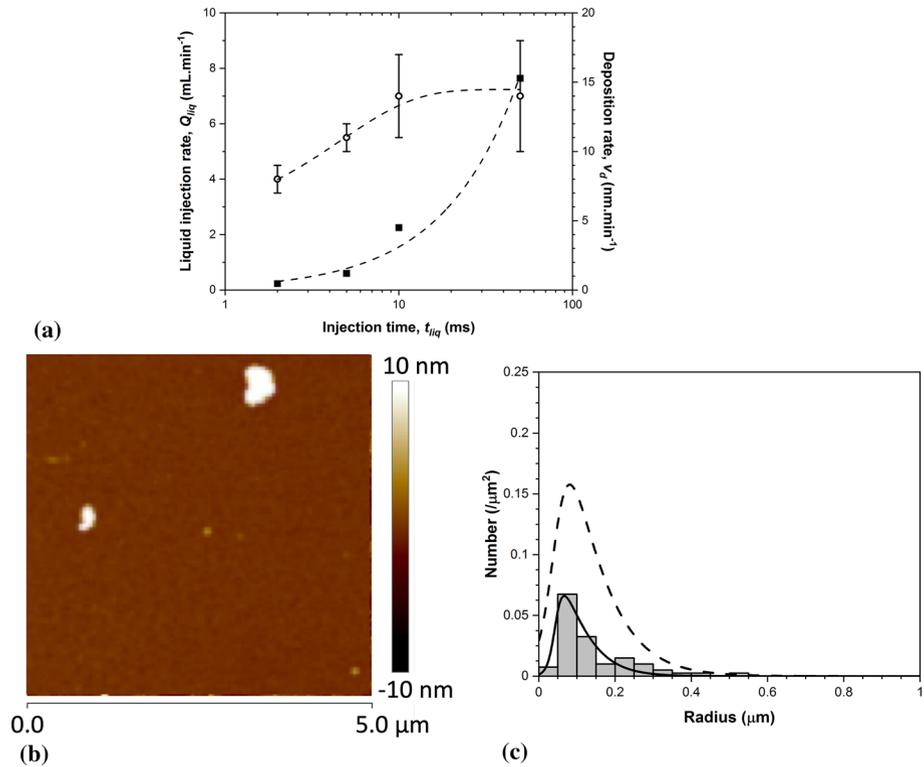
Fig. 8 **a** Variations of the liquid injection rate (squares) and deposition rate (open circles) as a function of the liquid opening time ($f=1$ Hz). **b** AFM images of the coatings obtained at $t_{liq}=2$ ms ($t_{gas}=10$ ms and $f=1$ Hz) and **c** the corresponding size distribution of the nano-objects (the dashed line correspond to the distribution defined in Fig. 2.c)

observed in every cases as, for example, for the coating deposited for $t_{liq}=2$ ms (Fig. 8b). However, though the size distribution, reported in Fig. 8c, does not significantly vary with a size distribution around 50–100 nm, it contains ≈ 2.5 times less nano-/micro-objects than on the coating deposited for $t_{liq}=5$ ms. The number of the defects looks directly controlled by the number of droplets injected per pulse. It suggests that the process involves droplets reactions in the plasma volume. Consequently, with the number of droplets, the plasma process may also be affected.

5.2 At the Pulse Scale

Figure 9 presents the profiles of working pressure (p_0 and p_{pulse}) and self-bias voltage ($V_{dc,0}$ and $V_{dc,pulse}$) as a function of liquid injection time. As shown in Fig. 9a, in contrast with the base pressure p_0 that exhibits slight variation over the t_{liq} range investigated herein, p_{pulse} and, consequently, Δp increase with the liquid injection time. However, the self-bias voltage $V_{dc,0}$ and $V_{dc,pulse}$ remain practically unchanged (Fig. 9b).

However, two regimes can be defined. From 2 to 10 ms, the pressure is roughly proportional to t_{liq} as reported in Fig. 9a. For example, in this range, p_{pulse} raises from 0.13 to 0.42 mbar thus increasing Δp by a factor of ≈ 4. This is not further the case above 10 ms
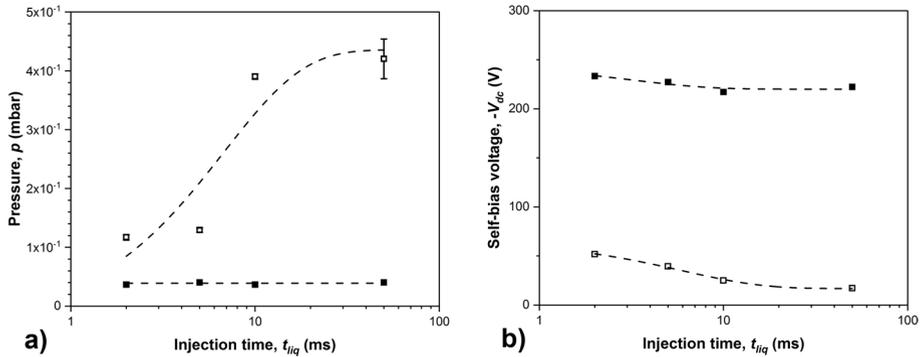
Fig. 9 Variation of **a** pressure and **b** self-bias voltage as a function of injection time ($f=1$ Hz). Open and full symbol correspond to respectively base and pulse pressure or bias voltage

where the pressure tends to saturate. Consequently, droplet evaporation appears directly correlated with the one of deposition rate observed on Fig. 8a.

The number of droplets is then controlling the vaporization of liquid droplets. This phenomenon has been reported, for example, in dense sprays where weak interactions (accumulation of vapors, cooling of the surrounding gas) can affect the evaporation rate [39] in contrast with dilute sprays where every droplet vaporizes as single isolated one. However, in terms of plasma physics, aerosol injection is smothering the discharge independently on the number of droplets.

Hence, regardless of the injection conditions, the main mechanism that controls the deposition process is droplet evaporation. Indeed, the deposition process is in every case limited by the production of neutral species from the liquid droplets. It means that the size and kinetics of liquid droplets must be carefully characterized to develop and optimize aerosol-assisted plasma processes.

Conclusion

In this study, we show that thin films are efficiently produced by pulsed aerosol injection in a low-pressure RF discharge. The PE-CVD process, including the aerosol characteristics and dynamics, are studied. They are directly controlled by the PDLI parameters. Especially, the material balance can be directly described, as classically in PE-CVD processes, as a function of power input per gas density. The injection frequency, f, affects the residence time of injected droplets, thereby influencing the density of neutral species formed by liquid evaporation as observed on the working pressures. Meanwhile, the amount of liquid injected per pulse or the number of injected droplets controlled by t_{liq}, have a negative effect on the liquid evaporation reducing the material balance. This study provides insight into the behavior of the plasma in the presence of pulsed aerosol injection: to optimize the deposition process in terms of mass balance, one would choose to inject a small quantity of droplet (lower f and t_{liq}), not to increase the ratio of power input with the flow rate, but to promote the mechanisms of liquid evaporation.

Declarations

Conflict of interest The authors declare no conflict of interest.

References

1. Biederman H, Slavínská D (2000) Surf Coat Technol 125(1–3):371–376
2. Hegemann D, Gaiser S (2021) J Phys D: Appl Phys 55(17):173002
3. Tachibana K, Nishida M, Harima H, Urano Y (1984) J Phys D: Appl Phys 17(8):1727
4. Von Keudell A, Möller W (1994) J Appl Phys 75(12):7718–7727
5. Clay K, Speakman S, Morrison N, Tomozeiu N, Milne W, Kapoor A (1998) Diam Relat Mater 7(8):1100–1107
6. Martinu L, Poitras D (2000) J Vac Sc Technol A: Vac Surf Films 18:2619–2645
7. Hassan MK, Pramanik BK, Hatta A (2006) Jpn J Appl Phys 45(10S):8398
8. Ravi N, Bukhovets V, Varshavskaya I, Sundararajan G (2007) Diam Relat Mater 16(1):90–97
9. Hegemann D (2006) Thin Solid Films 515(4):2173–2178
10. Andersson L, Berg S, Norström H, Olaison R, Towta S (1979) Thin Solid Films 63(1):155–160
11. Fourches N, Turban G (1996) Plasmas Polym 1(1):47–64
12. Fortov V, Ivlev A, Khrapak S, Khrapak A, Morfill G (2005) Phys Rep 421(1–2):1–103
13. C. Vahlas, H. Guillon, F. Senocq, B. Caussat, and S. Bonnafous, (2009) *Gases Instrum.*, pp. 8–11,
14. Capote G, Olaya J, Trava-Airoldi V (2014) Surf Coat Technol 251:276–282
15. Capote G, Silva G, Trava-Airoldi V (2015) Thin Solid Films 589:286–291
16. Chouquet C, Gerbaud G, Bardet M, Barrat S, Billard A, Sanchette F, Ducros C (2010) Surf Coat Technol 204(9–10):1339–1346
17. Andry P, Pastel P, Varhue W (1996) J Mater Res 11(1):221–228
18. Hormann C, Meier S, Moseler M (2009) Europ Phys J B 69:187–194
19. Schäfer J, Fricke K, Mika F, Pokorná Z, Zajíčková L, Foest R (2017) Thin Solid Films 630:71–78
20. Li D, Dai S, Goullet A, Granier A (2019) Plasma Process Polym 16(8):1900034
21. Suhr H (1989) Plasma Chem Plasma Process 9(1):7S-28S
22. Mitronika M, Granier A, Goullet A, Richard-Plouet M, Appl SN (2021) Sc 3(6):1–23
23. Mitronika M, Profili J, Goulet A, Gautier N, Stephant N, Stafford L, Granier A, Richard-Plouet M (2020) J Phys D: Appl Phys 54(8):085206
24. Profili J, Levasseur O, Blaisot J-B, Koronai A, Stafford L, Gherardi N (2016) Plasma Process Polym 13(10):981–989
25. Palumbo F, Lo Porto C, Fracassi F, Favia P (2020) Coatings 10(5):440
26. Ogawa D, Saraf I, Sra A, Timmons R, Goeckner M, Overzet L (2009) J Vac Sc & Technol A: Vac Surf, Films 27(2):342–351
27. M. Goeckner, D. Ogawa, I. Saraf, and L. Overzet, (2009) *J. Phys.: Conf. Series*, vol. 162, no. 1, pp. 012014
28. Cacot L, Carnide G, Kahn ML, Naudé N, Stafford L, Clergereaux R (2022) Plasma Process Polym 20(3):2200165
29. Carnide G, Cacot L, Champouret Y, Pozsgay V, Verdier T, Girardeau A, Cavarroc M, Sarkissian A, Mingotaud A-F, Vahlas C, Kahn ML, Naudé N, Safford L, Clergereaux R (2023) Coatings 13(3):630

30. Coppins M (2010) Phys Rev Lett 104(6):065003
31. Chouteau S, Mitronika M, Goullet A, Richard-Plouet M, Stafford L, Granier A (2022) J Phys D: Appl Phys 55(50):505303
32. Sadek T, Vinchon P, Durocher-Jean A, Carnide G, Kahn ML, Clergereaux R, Stafford L (2022) Atoms 10(4):147
33. Carnide G, Champouret Y, Valappil D, Vahlas C, Mingotaud A-F, Clergereaux R, Kahn ML (2023) Adv Sci 10(5):2204929
34. Berndt J, Kovačević E, Stefanović I, Stepanović O, Hong SH, Boufendi L, Winter J (2009) Contrib Plasma Phys 49(3):107–133
35. Takenaka K, Setsuhara Y (2019) Plasma Sources Sc Technol 28(6):065015
36. Cacot L, Carnide G, Kahn ML, Clergereaux R, Naudé N, Stafford L (2022) J Phys D: Appl Phys 55(47):475202
37. Hegemann D (2014) Comprehensive Mater Process 4:201–228
38. Lee C, Lieberman M (1995) J Vac Sc Technol A: Vac Surf Films 13(2):368–380
39. Shwin-Chung W, Jyh-Cheng C (1992) Intern J Heat Mass Transfer 35(10):2403–2411